Stress-hardening behaviour of biofilm streamers

Giovanni Savorana,[1] Tommaso Redaelli,[1] Domenico Truzzolillo, [2]
Luca Cipelletti, [2,3] Eleonora Secchi [1*]

[1]Department of Civil, Environmental and Geomatic Engineering,
ETH Zurich, Zurich, Switzerland
[2]Laboratoire Charles Coulomb (L2C), Université Montpellier, Montpellier, France
[3] Institut Universitaire de France, Paris, France

*To whom correspondence should be addressed; E-mail: esecchi@ethz.ch.

The natural environment exposes biological materials to diverse mechanical stimuli, requiring adaptive responses like stress-hardening to maintain structural integrity under varying stresses. While stress-hardening is well-documented in biological tissues, it remains understudied in bacterial biofilms. Here, we systematically demonstrate stress-hardening in biofilm streamers formed by clinically relevant bacterial species, using a microfluidic platform to perform *in situ* extensional rheological tests. Despite variations in matrix composition across species, DNA consistently emerges as a conserved and abundant component, indicating its role in inducing stress-hardening. Additionally, the biofilm matrix's viscoelastic properties exhibit a linear dependence on axial stress exerted by ambient flow, which we attribute to the entropic elasticity of DNA molecules. These findings provide critical insights into biofilms' mechanical resilience and adaptability upon exposure to flows.

Introduction

Many biological materials exhibit nonlinear mechanical properties that allow them to maintain structural integrity under varying mechanical stimuli. A prominent example of this is stress-hardening, a well-documented nonlinear property in biological tissues, characterized by increased stiffness in response to external loads. Notably, tissues become stiffer as the applied stress increases, enhancing their ability to withstand higher forces without sustaining damage (*1, 2*), a feature that plays a key role in cell migration, morphogenesis, organ development, and cancer progression (*3*). Recently, macroscopic stress-hardening in tissues has been linked to the entropic elasticity of single polymer chains embedded within their gel phases, which resist extension as conformational entropy decreases—a behaviour originally observed in polymers like DNA (*4–6*). While stress-hardening has been extensively studied in tissues, its role in biopolymer gels secreted by bacteria remains largely unexplored.

The production of cross-linked polymer gels is a crucial strategy used by bacteria to colonize their habitats. When transitioning from a planktonic to a sessile lifestyle, bacteria secrete extracellular polymeric substances (EPS) that self-assemble in the surrounding microenvironment, resulting in biofilm formation (*7–9*). Biofilms are widespread across various natural and artificial environments, and their viscoelastic mechanical properties significantly contribute to their ability to colonize and thrive (*10–14*). While viscoelasticity is a general property of biofilms, the extent to which they exhibit nonlinear mechanical behaviour remains unclear. Although stress-hardening has been observed in some biofilm studies (*15–17*), these observations remain isolated, and a systematic investigation of its dependence on EPS composition and environmental conditions is lacking. Given the crucial role of stress-hardening in biological tissues, this gap is notable, raising questions about its potential role in biofilm resilience and adaptability.

Streamers are thin, slender biofilm filaments that form on surfaces under fluid flow. They exemplify the ecological benefits of biofilm viscoelasticity, allowing them to withstand hydro-

dynamic stresses and extend far from colonized surfaces, thereby promoting bacterial spread (*18–21*). Streamer formation has been primarily studied in *Pseudomonas aeruginosa*, an important pathogen known for its role in chronic infections and recalcitrance to antibiotics, and a model organism for biofilm formation (*22–26*). Specifically, the PA14 strain produces streamers with a structural backbone composed of extracellular DNA (eDNA), while the polysaccharide Pel contributes to their morphology and mechanical properties (*20*). An eDNA backbone has also been reported in the streamers formed by *Burkholderia cenocepacia* (*27*). More broadly, eDNA is a key component of biofilms across various species, providing structural integrity to the extracellular matrix (*24, 28–33*). While eDNA chains and gels are known to exhibit stress-hardening behaviour (*34*), their contribution to nonlinear biofilm mechanics has yet to be explored.

Experimental setup and rheological characterization.

To systematically examine stress-hardening in the biofilm matrix, we use a microfluidic platform to grow biofilm streamers with a reproducible morphology from *P. aeruginosa* PA14 and PAO1, *B. cenocepacia*, *Staphylococcus epidermidis* and *Escherichia coli*, and characterize their material properties *in situ* (*21*). Pillar-shaped obstacles placed in a straight microfluidic channel act as nucleation points for pairs of biofilm streamers, which develop as millimetre-long filaments tethered to the sides of the pillars when a diluted bacterial suspension is flown through the channel. Once they reach a stable morphology, we perform extensional rheological measurements on nearly cell-free portions of a streamer, thus determining the viscoelastic properties of homogeneous EPS matrix samples. Since streamers develop under continuous background flow, they are constantly subjected to extensional axial stress (σ) and remain in a state of deformation with a non-zero extensional strain (ε). The axial stress at position x on a streamer of total length L depends on the surface area of the downstream portion of the streamer exposed

to flow and is expressed as:

$$\sigma\left(x\right) = \frac{1}{A(x)} \int_{x}^{L} \int_{0}^{2\pi} \left(\bar{\bar{\sigma}}(x',\,\theta) \cdot \hat{n}(x',\,\theta)\right) \cdot \hat{x}\, R(x')\, \mathrm{d}x'\, \mathrm{d}\theta, \tag{1}$$

where $A\left(x\right) = \pi R^2\left(x\right)$ is the cross-sectional area of the streamer at x, $\bar{\bar{\sigma}}$ is the Cauchy stress tensor of the fluid flowing past the streamer, $\hat{n}$ is the unit vector perpendicular to the streamer surface, and $\hat{x}$ is the unit vector in the x direction (*21*). Equation 1 shows that the axial stress $\sigma(x)$, at a given position x along the streamer, depends not only on the stress tensor of the fluid $\bar{\bar{\sigma}}$, which is proportional to the flow velocity, but also on the morphology of the portion of streamer downstream of x. To test the viscoelastic properties of the streamers, we apply a controlled flow perturbation that imposes an increase in extensional stress ($\Delta\sigma$), resulting in an additional filament deformation characterized by a strain increment ($\Delta\varepsilon$). From these increments, we calculate the incremental Young's modulus (E_{diff}) and effective viscosity (η), providing a detailed description of the streamers' material properties under stress. This differential testing method is analogous to the one implemented for characterizing the shear rheology of tissue gels (*4, 35*).

Ambient flow affects biofilm streamer morphology.

Since ambient flow controls streamer formation, we start by investigating how different flow velocities (U_{gr}) affect streamer morphology, biochemical composition, and rheological properties using *P. aeruginosa* PA14. We examine the adaptation of streamers to varying flows by comparing strains with different levels of Pel polysaccharide production: the wild-type (wt) strain, which produces Pel in response to external forces (*36, 37*), the Pel-deficient mutant (Δpel) and the Pel-overproducer (ΔwspF), which is locked in the active state of Pel production (*20*).

Microfluidic experiments reveal that *P. aeruginosa* PA14 forms biofilm streamers across a range of flow velocities spanning an order of magnitude within the laminar regime ($\mathrm{Re} \in$

$[0.02, 0.20]$, Table S1). After 15 hours, streamers formed under different velocities exhibit similar morphologies but vary in average length (L) and radius (R) (Fig. 1e-f). These differences are due to flow-induced changes in cell and EPS assembly rather than biomass flux, which we maintain constant across conditions (Methods). The average length notably decreases with increasing flow velocity, regardless of Pel production levels (Fig. 1e). Time-lapse imaging shows that higher velocities delay the formation of the first stable biofilm threads, likely due to reduced cell attachment, consistent with observations on flat surfaces (*38*) (Fig. S1a, b). After the initial time lag (t_0), the length increases with time approximately following a power law behaviour, $L \propto (t - t_0)^{0.5}$, under all flow conditions, with growth rates slower at higher velocities (Fig. S1c). Near the pillar (ROI_1, Fig. 1a, c), the radius increases significantly with flow velocity (Fig. 1f), while downstream (ROI_2, Fig. 1b, d), streamers are typically thinner, with the radius increasing with flow velocity for the wild-type strain, but showing no clear trends for the Pel-deficient and overproducer strains (Fig. 1f). Overall, these findings indicate that flow velocity significantly influences streamer development and morphology, with limited dependence on Pel polysaccharide abundance. It is important to highlight that the dependence of streamer morphology on ambient flow conditions implies that streamers grown at higher flow velocities are not necessarily subjected to higher extensional axial stresses, according to eq. 1.

Rheological characterization of streamers grown under different flow velocities.

Mechanical tests performed on PA14 biofilm streamers grown under different flow velocities reveal a linear relationship between the matrix viscoelastic properties and the axial stress exerted by the flow. We grow the biofilm streamers for 15 hours at a constant flow velocity, and then we characterize the rheology of specific portions. During the mechanical tests, we instantaneously double the initial flow velocity from $U_0 = U_{\mathrm{gr}}$ to $U_{\mathrm{cr}} = 2U_0$ (Fig. S2a). This increase

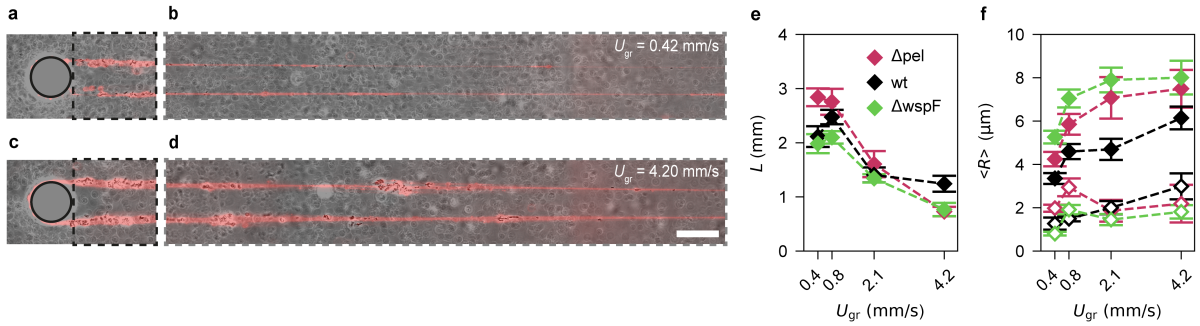

Figure 1: **The morphology of *P. aeruginosa* PA14 biofilm streamers is affected by ambient flow conditions during their growth**. **a-d**, Representative overlaid phase contrast and fluorescence images of 15-h-old PA14 wild-type biofilm streamers grown on a micropillar at the lowest ($U_{\mathrm{gr}} = 0.42$ mm/s, **a**, **b**), and highest ($U_{\mathrm{gr}} = 4.20$ mm/s, **c**, **d**) average flow velocities tested in this study. The flow is laminar, and the flux of bacterial cells is constant across the different flow conditions. The black and grey dashed rectangles highlight the regions corresponding to ROI_1 ($x \in [25\ \mu\mathrm{m}, 125\ \mu\mathrm{m}]$) and ROI_2 ($x \in [400\ \mu\mathrm{m}, 1065\ \mu\mathrm{m}]$), respectively. The scale bar is $50\ \mu\mathrm{m}$. Bacterial cells were imaged in phase contrast, and eDNA was stained using red-fluorescent propidium iodide ($2\ \mu\mathrm{g/mL}$). **e-f**, Averages length L (**e**) and average of $\langle R \rangle$ in ROI_1 (**f**, closed symbols) and ROI_2 (**f**, open symbols) as a function of the average flow velocity U_{gr} inside the microchannel during streamer formation for PA14 Δpel (magenta), wild-type (black) and ΔwspF (green). The error bars are the standard error of the mean.

results in an axial stress change on the examined portion of the streamer from the prestress value $\sigma_0 \equiv \langle \sigma(x; U_0) \rangle_{12}$ to the creep value $\sigma_{\mathrm{cr}} \equiv \langle \sigma(x; U_{\mathrm{cr}}) \rangle_{12}$ (Methods). Neglecting fluid-structure interaction (*21*), we have $\sigma_{\mathrm{cr}} = 2\sigma_0$ (Fig. S2b). The corresponding stress increment ($\Delta\sigma = \sigma_{\mathrm{cr}} - \sigma_0$) is maintained for $5\,\mathrm{min}$, during which we use optical microscopy to quantify the time-dependent strain increment ($\Delta\varepsilon\,(t)$) (Fig. S2c). Finally, we use $\Delta\sigma$ and $\Delta\varepsilon$ to determine the differential Young's modulus and effective viscosity of the sample portion under the prestress condition σ_0. Across a wide range of prestress conditions (Fig. S3), both the differential Young's modulus and effective viscosity exhibit an approximately linear correlation with the prestress ($E_{\mathrm{diff}} \propto \sigma_0^{0.99}$, $\eta \propto \sigma_0^{1.11}$) (Fig. 2).

The increase in differential Young's modulus with prestress maintains the elastic strain in-

crement below 10% across all tested conditions (Fig. S5a). By restricting deformation and preserving the structure of the bacterial community during mechanical challenges, the stress-hardening effect may provide a competitive ecological advantage in dynamic ecosystems by keeping community members within interaction distance. Given the critical role of interactions within bacterial communities, further studies are needed to explore this aspect (*39*).

The observed linear dependence of the differential Young's modulus and effective viscosity on the prestress is independent of the EPS matrix composition in PA14 biofilm streamers. First, this trend is not influenced by variations in eDNA density, as the density remains constant across a wide range of prestress conditions (Fig. S4). Second, the linear dependence observed in the PA14 Δpel strain indicates that Pel abundance does not determine this trend. Nevertheless, Pel abundance influences the viscoelastic properties, as shown previously (*20, 21*). For a given prestress, the Pel-overproducing strain consistently displays a higher differential Young's modulus than both the Pel-deficient and the wild-type strains, which show similar values (Fig. S5b, c). Pel staining reveals that in the wild-type strain, significant amounts of Pel are detected only near the pillar (ROI_1 in Fig S6a-d) at higher flow velocities ($U_{\mathrm{gr}} = 2.10\,\mathrm{ml/h}$ and $U_{\mathrm{gr}} = 4.20\,\mathrm{ml/h}$), while Pel concentration in the region where the mechanical properties are probed (ROI_2 in Fig. S6a-d) remains below our detection limit, regardless of flow velocity. Given that the viscoelastic properties of the EPS matrix correlate with the spatial distribution of polysaccharides within the biofilm (*40*), the similarity in the viscoelastic properties measured in both the wild-type and Pel-deficient mutants of the biofilm is consistent with the low levels of Pel polysaccharide found in the wild-type strain. In contrast, the ΔwspF mutant shows detectable Pel concentration in both ROI_1 and ROI_2 across all flow conditions, explaining its higher differential Young's modulus and effective viscosity compared to the other strains at a given prestress (Fig. S6e-h).

Given that the linear relationship between the viscoelastic properties and the prestress mea-

sured on streamers grown under different flow velocities cannot be attributed to flow-induced differences in EPS matrix composition, which are observed in surface-attached biofilms (*41*), we hypothesise that it may result from a nonlinear response of the matrix to mechanical stresses, as previously observed in biological networks formed from cytoskeletal and extracellular proteins (*4,6,35*). To validate this hypothesis, each streamer must be tested under multiple prestress conditions.

Stress-hardening behaviour in PA14 biofilm streamers.

By testing the rheology of each streamer under multiple prestress conditions, we demonstrate that the linear dependence of the viscoelastic properties on prestress results from the stress-hardening behaviour of the EPS matrix. To conduct the tests, we first grow PA14 streamers at $U_{\mathrm{gr}} = 2.10\ \mathrm{mm/s}$ for $15\ \mathrm{h}$. After this growth period, we perform two sequential mechanical tests on each sample. The tests are conducted using different initial flow velocities (U_0) for each test, with each U_0 having a corresponding creep velocity $U_{\mathrm{cr}} = 2U_0$. During the first test, the initial flow velocity is set to $U_0 = U_{\mathrm{gr}}$, which corresponds to a prestress of $\sigma_0 = \langle \sigma(x; U_{\mathrm{gr}}) \rangle_{12}$, as described in the previous paragraph. After the first test, we decrease the flow velocity to $U_{\mathrm{gr}}/5 = 0.42\ \mathrm{mm/s}$ and let the system stabilise for 10 minutes. Following this, we perform a second mechanical test with initial flow velocity $U_0 = U_{\mathrm{gr}}/5$, corresponding to a prestress $\sigma_0 = \langle \sigma(x; U_{\mathrm{gr}}/5) \rangle_{12}$ (Methods, Fig. S2). We image and analyzed the same portion of the streamer in both tests to determine the differential Young's modulus and effective viscosity of the same sample under the two different prestress conditions (Fig. S2d-f). In some selected experiments, we reverse the order of the mechanical tests to ensure that the observed viscoelastic properties are independent of the loading history, testing the streamer first under prestress $\sigma_0 = \langle \sigma(x; U_{\mathrm{gr}}/5) \rangle_{12}$ and then under prestress $\sigma_0 = \langle \sigma(x; U_{\mathrm{gr}}) \rangle_{12}$.

The differential Young's modulus and effective viscosity values measured sequentially on

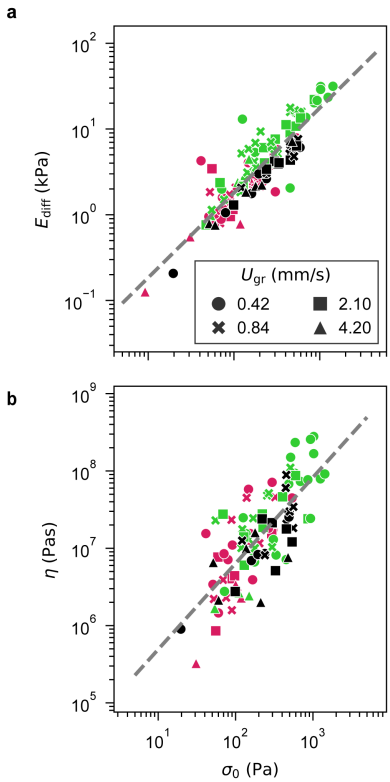

Figure 2: **The viscoelastic properties of *P. aeruginosa* PA14 biofilm streamers linearly depend on the prestess σ_0 exerted by U_{gr}. a, b**, Differential Young's modulus E_{diff} and effective viscosity η as a function of prestress σ_0. Each point is measured on a portion of a different streamer, whose prestress value $\sigma_0 = \langle \sigma(x; U_{\mathrm{gr}}) \rangle_{12}$ is determined by sample morphology and U_{gr}. Here, the notation $\sigma(x; U)$ is used to explicitly show the parametric dependence of the stress on flow velocity U. All samples are tested after $15\,\mathrm{h}$ of growth. Different colours represent the different PA14 mutants: Δpel (magenta), wild-type (black), and ΔwspF (green). Different symbols represent data points obtained for samples grown at different average flow velocities U_{gr}: $0.42\ \mathrm{mm/s}$ (circles), $0.84\ \mathrm{mm/s}$ (crosses), $2.10\ \mathrm{mm/s}$ (squares) and $4.20\ \mathrm{mm/s}$ (triangles). The dashed grey lines are power-law fits of the data, with exponent 0.99 ± 0.05 ($R^2 = 0.79$) with a 95% confidence interval $[0.90, 1.08]$ in **a** and 1.11 ± 0.10 ($R^2 = 0.56$) with a 95% confidence interval $[0.92, 1.31]$ in **b**.

the same sample exhibit the same linear dependence on prestress as in streamers grown under different ambient flow conditions (Fig. 2, 3). This trend is consistent across all PA14 mutants, regardless of their Pel polysaccharide production levels, and is, therefore, independent of Pel abundance. The 10-minute interval between the tests is sufficient for the system to stabilize at the new flow velocity but too brief for bacteria to initiate any adaptive mechanisms (*36*). Therefore, we conclude that the rheological adaptation of the streamer EPS matrix to the prestress is an instantaneous, purely mechanical stress-hardening response, which also explains the trends observed for streamers grown under different flow velocities (Fig. 2).

Given the dependence of viscoelastic properties on prestress, biofilm streamers should be compared based on tests conducted at a fixed prestress rather than a fixed flow velocity. This is demonstrated by the PA14 wild-type and Δpel streamers, which show no significant differences in the differential Young's modulus and effective viscosity when measured as a function of prestress, but show apparent differences when results are aggregated by flow conditions (Fig. S5b, c) (*20, 21*).

Stress-hardening behaviour in streamers across several bacterial species.

Experiments conducted with several widely spread bacterial species, common infection agents and model organisms for biofilm research, demonstrate that stress-hardening is a universal feature of the biofilm streamer EPS matrix. In these experiments, we grow streamers using suspensions of *P. aeruginosa* PAO1, *B. cenocepacia* H111, *S. epidermidis* 1457, and *E. coli* RP437, flowing at $U_{\mathrm{gr}} = 2.10\ \mathrm{mm/s}$ for $15\ \mathrm{h}$. These species differ in shape, motility and EPS components, with *S. epidermidis* being gram-positive and the others gram-negative bacteria (*42–46*). Despite these differences, all species form biofilm streamers with an eDNA backbone, morphologically similar to those produced by PA14 (Fig. 4a-d).

Sequential mechanical tests performed under different prestress, as in Fig. 3, reveal the same

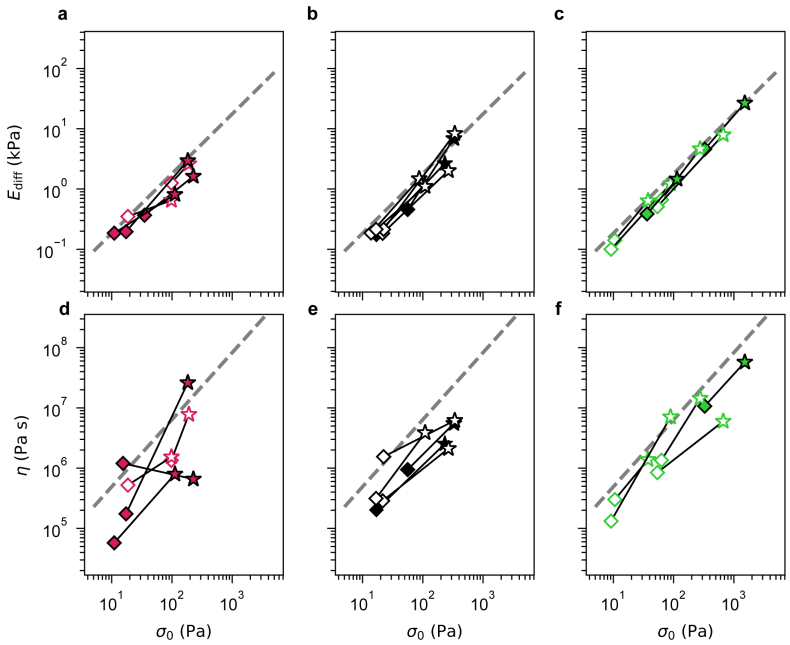

Figure 3: **The EPS matrix of *P. aeruginosa* PA14 biofilm streamers displays stress-hardening viscoelastic properties**. Differential Young's moduli E_{diff} (**a**-**c**) and effective viscosities η (**d**-**f**), obtained from two sequential mechanical tests performed on the same portion of the streamer, demonstrate the stress-hardening behaviour of the streamer matrix of PA14 Δpel (**a**, **d**, magenta), wild-type (**b**, **e**, black), and ΔwspF (**c**, **f**, green). Each pair of markers connected by a solid line represents values measured on the same sample under two different prestress conditions σ_0. The tests are conducted on PA14 biofilm streamers grown for $15\,\mathrm{h}$ at an average flow velocity $U_{\mathrm{gr}} = 2.10\ \mathrm{mm/s}$. The tests of each pair are conducted with initial flow velocities $U_0 = U_{\mathrm{gr}} = 2.10\ \mathrm{mm/s}$ (stars) and $U_0 = U_{\mathrm{gr}}/5 = 0.42\ \mathrm{mm/s}$ (diamonds). The corresponding prestress values are $\sigma_0 = \langle \sigma(x; U_{\mathrm{gr}}) \rangle_{12}$ and $\sigma_0 = \langle \sigma(x; U_{\mathrm{gr}}/5) \rangle_{12}$. Open symbols mark data measured first at $U_0 = U_{\mathrm{gr}}$ and then $U_0 = U_{\mathrm{gr}}/5$, while closed symbols are measured at $U_0 = U_{\mathrm{gr}}/5$ and then at $U_0 = U_{\mathrm{gr}}$. The dashed grey lines in **a**-**c** and **d**-**f** are the power law fits of the data reported in Fig. 2a and b, respectively. We verified that the observed strain-hardening behaviour is not significantly altered if fluid-structure interaction is accounted for in the calculation of the streamer rheology (Figure S9).

stress-hardening behaviour observed in PA14 streamers (Fig. 4e-h). Specifically, the differential Young's modulus of the streamers from all tested species scales linearly across a wide range of prestress, spanning nearly three orders of magnitude (Fig. 4i). Moreover, the prefactor also remains consistent across the testing conditions and different bacterial species. The consistent stress-hardening behaviour and linear scaling observed across different species, combined with the presence of eDNA as a common and abundant component in their EPS matrices, indicates a link between this stress-hardening and the mechanical properties of the eDNA backbone.

To explore this hypothesis, we modelled the expected elastic response of a DNA network under uni-axial extension using a framework based on the worm-like chain model (*47*) and parameters to describe the eDNA that are consistent with literature values (*33*) (Supplementary Information). This model accounts for the entropic elasticity of DNA molecules and was previously applied to describe the strain-hardening behaviour in DNA gels under shear (*48, 49*). In the uni-axial extension configuration tested in our experiments, the model predicts three regimes: a linear elastic regime at low prestress, where E_{diff} is constant, a crossover regime at intermediate prestress where $E_{\text{diff}} \propto \sigma_0$ and a regime at large prestress where $E_{\text{diff}} \propto \sigma_0^{1.5}$. Notably, this predicted crossover regime overlaps with the range of prestress observed in our experiments, assuming high DNA densities ($n \approx 10^{21}\, m^{-3}$) and a contour length of DNA chains between neighbouring cross-links $L_c \geq 50\,\mu\text{m}$ (Supplementary Materials, Fig. S10). Although definitive proof will require experimental characterization of DNA density and matrix mesh size, the strong alignment between the experimental data and the model suggests that the stress-hardening behaviour of streamers has an entropic origin emerging from the mechanical properties of eDNA.

Previous studies have suggested that specific polysaccharides are required for the EPS matrix to withstand large stresses without rupturing, but they have not attributed this resilience to nonlinear mechanical behaviours (*50*). While some research has observed nonlinear mechanical

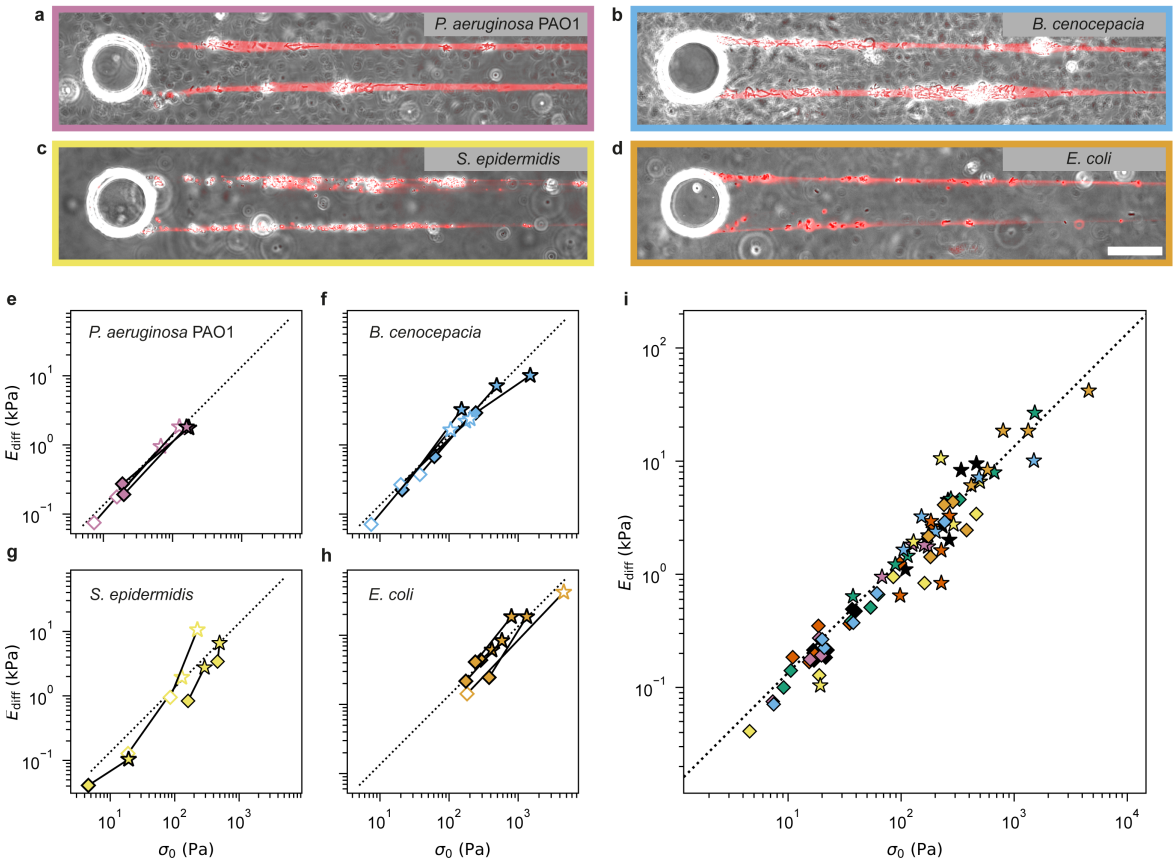

Figure 4: **The stress-hardening behaviour of the EPS matrix is consistent across biofilm streamers from several bacterial species**. **a-d**, Representative overlaid phase contrast and fluorescence images of portions of biofilm streamers grown for $15\,\mathrm{h}$ at an average ambient flow velocity of $U_{\rm gr} = 2.10\ \mathrm{mm/s}$ by *P. aeruginosa* PAO1 (**a**), *B. cenocepacia H111* (**b**), *S. epidermidis* 1457 (**c**), and *E. coli* RP437 (**d**). The scale bar is 50 µm. **e-h**, Differential Young's moduli $E_{\rm diff}$, obtained from sequential mechanical tests, as a function of the axial stress σ_0, demonstrating the stress-hardening behaviour of biofilm streamers formed by *P. aeruginosa* PAO1 (**e**), *B. cenocepacia* H111 (**f**), *S. epidermidis* 1457 (**g**), and *E. coli* RP437 (**h**), grown at average flow velocity $U_{\rm gr} = 2.10\ \mathrm{mm/s}$. Solid lines connect results from the same portion of the streamer tested under two axial stress conditions σ_0. Tests are conducted on 15-hour-old streamers with initial flow velocity $U_0 = U_{\rm gr} = 2.10\ \mathrm{mm/s}$ (stars) and $U_0 = U_{\rm gr}/5 = 0.42\ \mathrm{mm/s}$ (diamonds). Corresponding prestress values are $\sigma_0 = \langle\sigma(x; U_{\rm gr})\rangle_{12}$ and $\sigma_0 = \langle\sigma(x; U_{\rm gr}/5)\rangle_{12}$. Open symbols indicate data measured first at the higher and then lower σ_0 values, while closed symbols are measured at the lower and then at the higher σ_0 values. **i**, Scatterplot of the values reported in panels **a-c** of Fig. 3 and panels **e-h** of this figure (same colour code of the original panels). The dotted lines in panels **e-i** indicate a power law behaviour with an exponent of 1.

properties in biofilms, the specific EPS components responsible for the nonlinearity have not been identified or hypothesized (*51, 52*). Our study indicates that eDNA confers these nonlinear properties. Over the past two decades, eDNA has evolved from being considered a minor component to being recognized as a critical structural element of biofilms (*20, 28, 32, 33, 53, 54*). In addition, eDNA can protect bacterial communities within biofilms from antimicrobials and antibiotics (*55, 56*), and human DNA released during infection or environmental DNA can also be integrated into biofilms (*57, 58*). Together with our results, these findings suggest that DNA plays a significant role in shaping biofilm structure and governing their nonlinear rheological behaviour. The widespread presence of eDNA in biofilms implies that stress-hardening behaviour may be more prevalent than previously indicated by often contradictory experimental and modelling results (*51, 52*). Therefore, our study prompts a reconsideration of the role of eDNA in biofilm structuring and offers a promising framework for testing hypotheses on the microscopic mechanisms underlying biofilm rheology.

In summary, the stress-hardening of biofilms has rarely been experimentally observed and has never been systematically investigated in previous studies, leaving a critical gap in our understanding of its potential relevance for biofilm formation, ecology, and eradication. Here, we use microfluidics to grow and test biofilm streamers *in situ* and determine the mechanical properties of the biofilm matrix of *P. aeruginosa*, *B. cenocepacia*, *S. epidermidis* and *E. coli* strains. Our findings consistently demonstrate significant stress-hardening behaviour in biofilm streamers subjected to extensional axial stress, where the differential Young's modulus and effective viscosity scale linearly with prestress. The good agreement between the experimental data and the model of a DNA network's elastic response under uniaxial extension indicates that the stress-hardening behaviour of streamers is of entropic nature, stemming from the mechanical properties of eDNA. Entropic elasticity contributes to the stress-hardening of biological networks such as actin, vimentin and neurofilament networks (*4, 5*). In these gels, which consti-

tute biological tissues, the increase in the differential Young's modulus is comparable to what we observed for biofilm streamers. Thus, our findings suggest that eDNA not only serves as a fundamental structural element of streamers (*20*), but also imparts strong stress-hardening behaviour. This likely enables streamers to adapt instantaneously to fluctuating mechanical forces in their environments, similar to the adaptive behaviour observed in biological tissues.

References

1. M. G. Wertheim, *Annal. Chim. Phys.* **21**, 385 (1847).
2. C. F. Guimarães, L. Gasperini, A. P. Marques, R. L. Reis, *Nat. Rev. Mater.* **5**, 351 (2020).
3. B. Corominas-Murtra, N. I. Petridou, *Front. Phys.* **9** (2021).
4. M. L. Gardel, *et al.*, *Science* **304**, 1301 (2004).
5. Y.-C. Lin, *et al.*, *Phys. Rev. Lett.* **104**, 058101 (2010).
6. C. Storm, J. J. Pastore, F. C. MacKintosh, T. C. Lubensky, P. A. Janmey, *Nature* **435**, 191 (2005).
7. H.-C. Flemming, J. Wingender, *Nat. Rev. Microbiol.* **8**, 623 (2010).
8. P. Watnick, R. Kolter, *J. Bacteriol.* **182**, 2675 (2000).
9. G. O'Toole, H. B. Kaplan, R. Kolter, *Annu. Rev. Microbiol.* **54**, 49 (2000).
10. B. W. Peterson, *et al.*, *FEMS Microbiol. Rev.* **39**, 234 (2015).
11. E. S. Gloag, S. Fabbri, D. J. Wozniak, P. Stoodley, *Biofilm* **2**, 100017 (2020).
12. M. Caldara, C. Belgiovine, E. Secchi, R. Rusconi, *Clin. Microbiol. Rev.* **35**, e0022120 (2022).

13. A. Persat, *et al.*, *Cell* **161**, 988 (2015).

14. S. G. V. Charlton, *et al.*, *J. Bacteriol.* **201**, 10.1128/jb.00101 (2019).

15. P. Stoodley, R. Cargo, C. J. Rupp, S. Wilson, I. Klapper, *J. Ind. Microbiol. Biotechnol.* **29**, 361 (2002).

16. S. Grumbein, M. Werb, M. Opitz, O. Lieleg, *J. Rheol.* **60**, 1085 (2016).

17. J. N. Wilking, T. E. Angelini, A. Seminara, M. P. Brenner, D. A. Weitz, *MRS Bull.* **36**, 385 (2011).

18. R. Rusconi, S. Lecuyer, N. Autrusson, L. Guglielmini, H. A. Stone, *Biophys. J.* **100**, 1392 (2011).

19. K. Drescher, Y. Shen, B. L. Bassler, H. A. Stone, *Proc. Natl. Acad. Sci. U.S.A.* **110**, 4345 (2013).

20. E. Secchi, *et al.*, *Proc. Natl. Acad. Sci. U.S.A.* **119**, e2113723119 (2022).

21. G. Savorana, J. Słomka, R. Stocker, R. Rusconi, E. Secchi, *Soft Matter* **18**, 3878 (2022).

22. M. F. Moradali, S. Ghods, B. H. A. Rehm, *Front. Cell. Infect. Microbiol.* **7**, 39 (2017).

23. O. Ciofu, C. Moser, P. Ø. Jensen, N. Høiby, *Nat. Rev. Microbiol.* **20**, 621 (2022).

24. L. K. Jennings, *et al.*, *Proc. Natl. Acad. Sci. U.S.A.* **112**, 11353 (2015).

25. L. Friedman, R. Kolter, *J. Bacteriol.* **186**, 4457 (2004).

26. L. Friedman, R. Kolter, *Mol. Microbiol.* **51**, 675 (2004).

27. Z. Heredia-Ponce, *et al.*, *npj Biofilms Microbiomes* **9**, 96 (2023).

28. C. B. Whitchurch, T. Tolker-Nielsen, P. C. Ragas, J. S. Mattick, *Science* **295**, 1487 (2002).

29. M. Allesen-Holm, *et al.*, *Mol. Microbiol.* **59**, 1114 (2006).

30. T. Seviour, *et al.*, *npj Biofilms Microbiomes* **7**, 27 (2021).

31. A. Devaraj, *et al.*, *Proc. Natl. Acad. Sci. U.S.A.* **116**, 25068 (2019).

32. J. R. Buzzo, *et al.*, *Cell* **184**, 5740 (2021).

33. S. Mugunthan, *et al.*, *Nat. Commun.* **14**, 7772 (2023).

34. J. F. Marko, E. D. Siggia, *Macromolecules* **28**, 8759 (1995).

35. A. J. Licup, *et al.*, *Proc. Natl. Acad. Sci. U.S.A.* **112**, 9573 (2015).

36. C. A. Rodesney, *et al.*, *Proc. Natl. Acad. Sci. U.S.A.* **114**, 5906 (2017).

37. J. W. Hickman, D. F. Tifrea, C. S. Harwood, *Proc. Natl. Acad. Sci. U.S.A.* **102**, 14422 (2005).

38. S. Lecuyer, *et al.*, *Biophys. J.* **100**, 341 (2011).

39. D. C. Alma, v. V. Simon, J. K. Daniel, S. Susan, A. Martin, *Nat. Ecol. Evol.* **4**, 165 (2020).

40. T. Ohmura, *et al.*, *Adv. Mater.* p. 2314059 (2024).

41. R. Hartmann, *et al.*, *Nat. Phys.* **15**, 251 (2019).

42. K. M. Colvin, *et al.*, *PLoS Pathog.* **7**, 1 (2011).

43. L. A. Novotny, A. O. Amer, M. E. Brockson, S. D. Goodman, L. O. Bakaletz, *PloS One* **8** (2013).

44. L. Chiarini, *et al.*, *J. Cyst. Fibros.* **3**, 165 (2004).

45. K. Schilcher, A. R. Horswill, *Microbiol. Mol. Biol. Rev.* **84**, 10.1128/mmbr.00026 (2020).

46. D. A. Hufnagel, W. H. Depas, M. R. Chapman, *Microbiol. Spectr.* **3** (2015).

47. R. W. Ogden, G. Saccomandi, I. Sgura, *Proc. R. Soc. A: Math. Phys. Eng. Sci.* **462**, 749 (2006).

48. C. Bustamante, J. F. Marko, E. D. Siggia, S. Smith, *Science* **265**, 1599 (1994).

49. N. Orakdogen, B. Erman, O. Okay, *Macromolecules* **43** (2010).

50. S. C. Chew, *et al.*, *mBio* **5**, 10.1128/mbio.01536 (2014).

51. C. Laspidou, L. Spyrou, N. Aravas, B. Rittmann, *Math. Biosci.* **251**, 11 (2014).

52. P. Barai, A. Kumar, P. P. Mukherjee, *PloS One* **11**, 1 (2016).

53. V. Dengler, L. Foulston, A. S. DeFrancesco, R. Losick, *J. Bacteriol.* **197**, 3779 (2015).

54. K. Schwartz, M. Ganesan, D. E. Payne, M. J. Solomon, B. R. Boles, *Mol. Microbiol.* **99**, 123 (2016).

55. W.-C. Chiang, *et al.*, *Antimicrob. Agents Chemother.* **57**, 2352 (2013).

56. H. Mulcahy, L. Charron-Mazenod, S. Lewenza, *PLoS Pathog.* **4**, 1 (2008).

57. H. Panlilio, C. V. Rice, *Biotechnol. Bioeng.* **118**, 2129 (2021).

58. M. Alhede, *et al.*, *Pathog. Dis.* **78** (2020).

59. E. M. Arruda, M. C. Boyce, *Journal of the Mechanics and Physics of Solids* **41**, 389 (1993).

60. N. Scott, *Mathematics and Mechanics of Solids* **12**, 526 (2007).

Acknowledgments

We thank Prof. Leo Eberl, Prof. Jan Vermant, Dr. Sam Charlton and Dr. Steffen Geisel for the insightful discussions; Prof. Leo Eberl for providing the *B. cenocepacia* strain and Prof. Paul D. Fey for the *S. epidermidis* strain; Ela Burmeister for the technical support; and support from the Swiss National Science Foundation PRIMA Grant 179834 (to E.S.) and the Institut Universitaire de France (L.C.). Finally, we acknowledge and honour the memory of Prof. Paul Stoodley, whose pioneering work in streamer formation and rheology has greatly influenced and inspired this research.